CHALMERS
UNIVERSITY OF TECHNOLOGY

Penetration of corrosive species into copper exposed to simulated O<inf>2</inf>-free groundwater by time-of-flight secondary ion mass

Downloaded from: https://research.chalmers.se, 2025-12-04 16:04 UTC

Citation for the original published paper (version of record):
Yue, X., Malmberg, P., Isotahdon, E. et al (2023). Penetration of corrosive species into copper exposed to simulated O<inf>2</inf>-free
groundwater by time-of-flight secondary ion mass spectrometry (ToF-SIMS). Corrosion Science, 210. http://dx.doi.org/10.1016/j.corsci.2022.110833

N.B. When citing this work, cite the original published paper.

research.chalmers.se offers the possibility of retrieving research publications produced at Chalmers University of Technology. It covers all kind of research output: articles, dissertations, conference papers, reports etc. since 2004. research.chalmers.se is administrated and maintained by Chalmers Library

(article starts on next page)

Corrosion Science 210 (2023) 110833

Contents lists available at ScienceDirect

Corrosion Science

journal homepage: www.elsevier.com/locate/corsci

Penetration of corrosive species into copper exposed to simulated O_2-free groundwater by time-of-flight secondary ion mass spectrometry (ToF-SIMS)

Xiaoqi Yue [a], Per Malmberg [b], Elisa Isotahdon [c], Vilma Ratia-Hanby [c], Elina Huttunen-Saarivirta [c], Christofer Leygraf [a], Jinshan Pan [a,*]

[a] Div. of Surface and Corrosion Science, Dept. of Chemistry, KTH Royal Institute of Technology, Stockholm, Sweden
[b] Dept. of Chemistry and Chemical Engineering, Chalmers University of Technology, Gothenburg, Sweden
[c] VTT Technical Research Centre of Finland Ltd., Espoo, Finland

ARTICLE INFO

Keywords:
Copper
Anoxic corrosion
Sulfide
ToF-SIMS
Nuclear waste

ABSTRACT

ToF-SIMS analysis of copper samples after exposures to simulated groundwater with and without sulfide addition was performed to investigate the penetration of corrosive species containing H, S, O, and Cl, into copper. Depth profiles show extent of penetration and 2D/3D images reveal local elemental distribution of the corrosive species at different depths inside copper. Pre-oxidation did not reduce the penetration while sulfide additional in groundwater and exposure at 60 °C significantly promoted the penetration. The extent of penetration of the corrosive species into copper demonstrates the need for risk assessment of complex corrosion forms such as sulfide-induced embrittlement and cracking.

1. Introduction

Spent fuel from nuclear power plants is highly radioactive and its safe disposal is as important as nuclear power plant safety. Governmental regulations require safe isolation of nuclear waste for a minimum of 100,000 years, which imposes a great engineering challenge. The nuclear waste disposal concept in Sweden and Finland is based on a three-barrier system, where the spent fuel is placed in cast-iron inserts, which are then sealed in copper canisters as the first barrier. The canisters are surrounded by a bentonite clay layer as the second barrier, further placed in bedrock (third barrier) in the depth of 400–1000 m [1,2]. High-purity oxygen-free phosphorus-containing copper (OFP-Cu) has been chosen for fabricating the canisters that will be placed in granite environments under anaerobic reduction and anoxic aqueous conditions. The bentonite clay is a buffer material between the bedrock and the canisters, swelling when exposed to water and thus dampening minor movements within the repository system, and retaining eventual release of radioactive nuclides upon possible canister failure. The bedrock provides the outermost barrier between the nuclear waste and the biosphere [1,2].

During long-term storage in the repository of the Cu canisters, cracks in the bedrock and the swelling of bentonite by groundwater lead to a direct contact of the Cu canisters with groundwater and the microbes in it. The groundwater contains a high level of Cl^- and SO_4^{-2} ions, and microbiological activity in the vicinity or on the surface of the canister produces sulfide species (mainly HS^- ions) [3–6]. Trapped O_2 exists in the system during initial period of the repository closure, but is gradually consumed by oxidation reactions and microorganisms. Once the trapped O_2 is completely consumed, the major threat to the long-term durability of the canister is corrosion by sulfide species (e.g., HS^-) produced in the groundwater by microbial activity and/or mineral dissolution. Microbial activity has been reported to initiate and accelerate general and localized corrosion of Cu, and cause a biotically-induced formation of a Cu_2S layer [3–7]. Corrosion of Cu under oxic and anoxic conditions, and the influence of radiation and microbiological activity, have been investigated, often separately, over 40 years [8–13]. Studies of Cu corrosion were often focused on chemical and electrochemical degradation of copper at the electrolyte/metal interface, and analysis of the corrosion products formed on the surface [14,15]. Chemical conversion of a native Cu_2O film to Cu_2S on the surface has been observed [16], and S-induced corrosion detected down to the depth of 100 nm into the Cu material [17]. At atomic level, the dissociation of sulfide species on the Cu surface is a spontaneous process, releasing atomic S and H. The co-existence with S promotes the H adsorption into copper according to DFT calculations [18,19]. Moreover, sulfide-induced corrosion reactions can generate H on the Cu

* Corresponding author.
E-mail address: jinshanp@kth.se (J. Pan).

https://doi.org/10.1016/j.corsci.2022.110833
Received 16 September 2022; Received in revised form 8 November 2022; Accepted 14 November 2022
Available online 21 November 2022
0010-938X/© 2022 The Author(s). Published by Elsevier Ltd. This is an open access article under the CC BY license (http://creativecommons.org/licenses/by/4.0/).

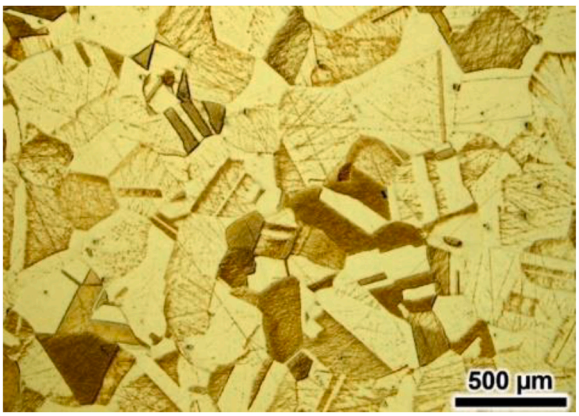

Fig. 1. Optical micrograph of an etched OFP-Cu material showing typical microstructure with large grains (of different crystallographic orientations) and annealing twins [19]. Thin lines show grinding scratches where plastic deformation exist.

surface [14]. Atomic H can also be produced at the water/Cu interface through radiolysis of water, and gamma radiation from spent nuclear fuel greatly increases the H generation on Cu, up to several orders of magnitude depending on the dose of the radiation [12,13]. In general, H has detrimental effects on the mechanical properties of Cu and can create voids and microcracks in Cu materials [20–23]. Adsorption and diffusion of H in Cu depend on the surface condition and presence of microstructural defects, such as dislocations and inclusions, and grain boundaries are the primary trapping sites of H [24]. In the Cu microstructure, H-induced lattice deformations may be heterogeneous, giving rise to local strains and stresses. Therefore, H incorporation into Cu can lead to the formation of a macroscopic lattice expansion, especially when accumulated in the surface region. H-induced strain localization has been observed in Cu in the initial stage of plastic deformation [25], and friction stir welding to seal the canister was found to increase H uptake in the weld zone and lead to strain localization around it [26]. H incorporation into Cu material leads to accelerated creep and the formation of microcracks with an intergranular nature [27]. H-induced damage of Cu canister has, so far, been considered to be negligible due to the belief that the H permeation depth would be too small to influence the mechanical integrity of Cu canister [28,29]. However, in the presence of tensile strains, sulfide has been shown to cause stress corrosion cracking (SCC) of Cu in anaerobic chloride containing environments [10,11,30].

A recent review gives an overview of the corrosion issues, debated questions, and ongoing research programs [6]. The corrosion of Cu canister has been assessed under expected repository conditions using a uniform corrosion rate to calculate the corrosion allowance [6]. However, the risks for several complex forms of Cu corrosion have been debated for a long time, even in the Land and Environmental Court of Sweden, which concluded that further information is needed regarding five issues: *i*) corrosion due to reaction in O_2-free water; *ii*) pitting due to reaction with sulfide; *iii*) SCC due to reaction with sulfide; *iv*) hydrogen embrittlement (HE); *v*) the effect of radioactive radiation on pitting, SCC and HE. Swedish Nuclear Fuel and Waste Management Co (SKB) has addressed these issues in an official report [31]. However, there are still intensive debates about these issues in Sweden [19,32,33]. Earlier in 2022, the Swedish government made a decision allowing SKB to start the long process preparing for the final disposal, meanwhile requesting regular revisions of the safety risk assessment of the system and eventual improvement. Clearly, there is a need to gain a deep understanding of the roles of H, S, O, and Cl in SCC and HE of Cu during the long exposure to the groundwater containing sulfide. This requires the detection of penetration and distribution of these corrosive species into the Cu microstructure. In this work, we utilized time-of-flight secondary ion mass spectroscopy (ToF-SIMS) to reveal the penetration of H, S, O, and Cl into Cu caused by the exposure to a O_2-free simulated groundwater with and without additional sulfide. This communication is focused on the ToF-SIMS results and their implications in nuclear waste disposal context.

2. Experimental

2.1. Sample preparation and exposure to simulated groundwater

Hot-rolled OFP-Cu, the material for making the canister, was used as the material for the experiments. The OFP-Cu was provided by Posiva Oy, Finland. The copper material had a typical hot-rolled microstructure, with large grains (from several tens to hundreds of micrometres in size) and annealing twins, see Fig. 1. Two initial conditions were used in the long exposure experiments: (*i*) the polished Cu surface, and (*ii*) pre-oxidised Cu surface that was after equal grinding exposed for seven days to air at the temperature of 90 °C. The samples had the dimensions of 10 mm × 10 mm × 3 mm, the surface was wet-ground down to 600 grits, and cleaned in acetone and ethanol prior to the exposure. The pre-oxidation was done to simulate the effect of initial oxic conditions at the elevated temperature on Cu, prior to anoxic phase in disposal. The elevated temperature was chosen to take into account the effect of radiation from the spent fuel. Highly radioactive nuclear waste repositories may exhibit significant temperature variations depending on their location, time, and type of waste, a temperature increase up to 90 °C is predicted within 10–30 years after closure, followed by a slow temperature decrease to natural condition in thousands of years [6,8].

The exposures were conducted at VTT using simulated groundwater with and without additional sulfide. Table 1 gives the chemical composition of the groundwater, which was derived based on the groundwater chemistry of the planned disposal site and the effect of ion exchange with the bentonite. The sulfide was added in the form of Na_2S. Besides sulfide addition, the groundwater contains a high level of chloride and sulphate ions. The experiments were mostly conducted at room temperature (22 °C) in glass vessels, while some samples were exposed at 60 °C in glass vessels placed in a heat chamber. The test vessels were gas-tight laboratory glass bottles with the volume of 5 L. The experiments were carried out in anoxic environment: the water and vessels were flushed with argon before the start of the tests. Vessels were sealed with butyl rubber stoppers to prevent O_2 contamination during the experiment. Redox potential monitoring and chemical analysis of the groundwater were performed to verify that anoxic nature of test system was maintained over the test duration. The exposure at 60 °C was done replicating the period of increased temperature in the early period of disposal. After the exposure, the samples were dried in air and then stored in desiccator. Exposure runs with different levels of added Na_2S and time durations, electrochemical measurements and characterization of the corrosion products were reported in the final project report [34]. The samples after exposure to the groundwater without/with 0.001 M (32 mg/L) Na_2S addition were chosen for ToF-SIMS analysis.

Table 1
The chemistry of the simulated groundwater, to which 0.001 M Na_2S was added.

	K	Ca	Cl	Na*	SO_4	Br	HCO_3	Mg	Sr	Si	B	F	Mn	PO_4	lactate
mg/L	54.7	280.0	5274.0	3180.2	595.0	42.3	13.7	100.0	8.8	3.1	1.1	0.8	0.2	0.1	1

* Original Na content; actual amount also includes the addition of Na_2S.

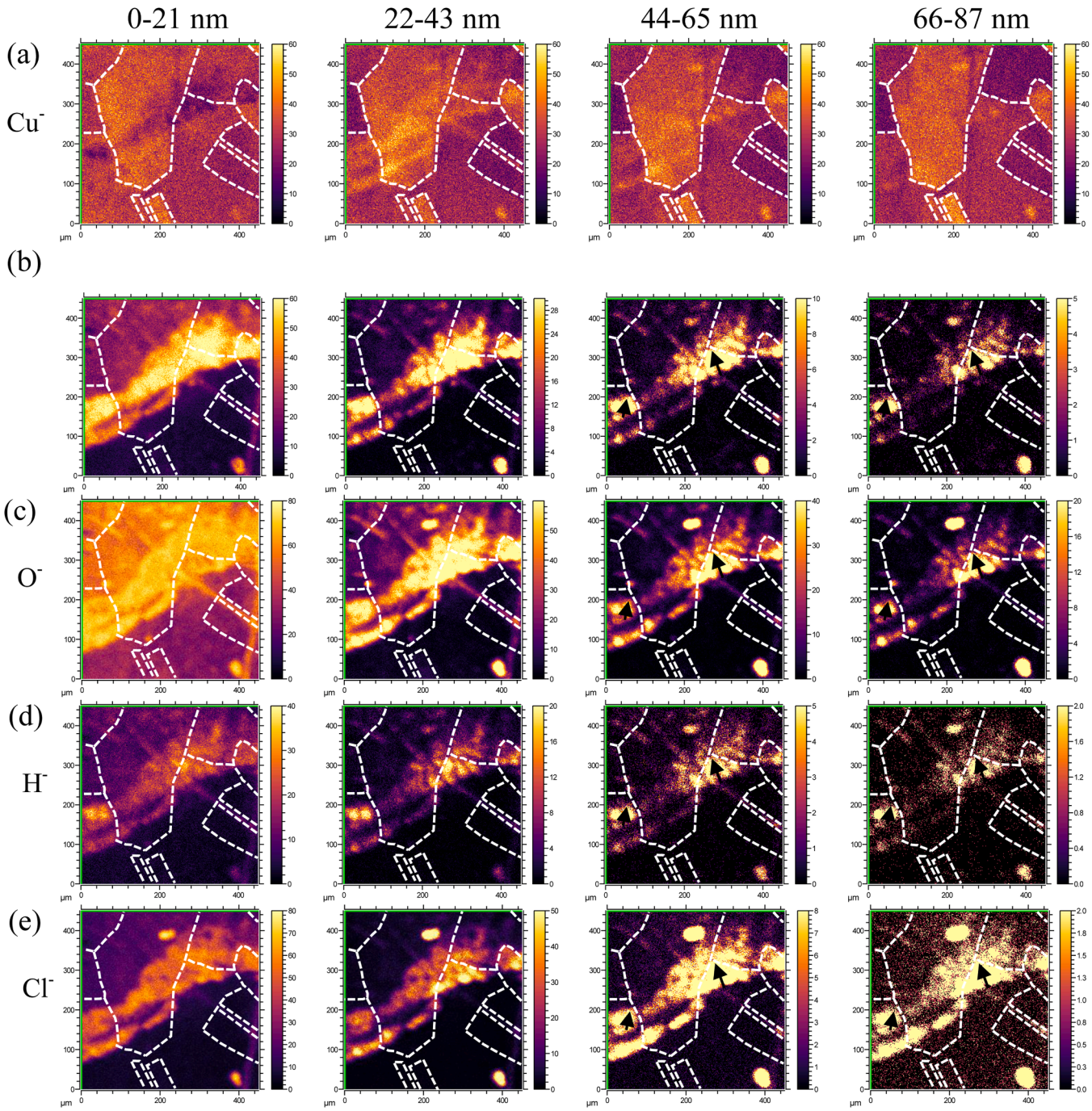

Fig. 2. Plane views by ToF-SIMS analyses at different depth intervals (0–21, 22–43, 44–65 and 66–87 nm) of a polished Cu sample after 9-month exposure in the simulated groundwater without Na_2S, at ambient temperature. (a) Cu^-, (b) S^-, (c) O^-, (d) H^-, and (e) Cl^-. The field of view is 450 µm × 450 µm. Arrows mark the segregation along the grain boundaries.

2.2. ToF-SIMS measurements

ToF-SIMS analyses were performed for selected Cu samples after the exposure. Before the analysis, the exposed samples were stored in desiccator for a long time: 1 year for the 9-month exposed samples and 0.5 year for the 4-month exposed samples. ToF-SIMS techniques including depth profiling and 2D/3D imaging, and their applications in material science have been described in literature [35–38]. ToF-SIMS has been extensively used to study high temperature oxidation mechanisms of alumina formers [39,40] and corrosion processes of engineering alloys [41–43]. In two SKB reports, ToF-SIMS measurements were included in the study of corrosion of Cu in O_2-free pure water, however, only depth profiles were briefly discussed regarding the estimate the thickness of the oxide film, while no 2D/3D imaging was made to map the distribution of the corrosive species inside the Cu metal [44,45]. In our work, ToF-SIMS measurements were performed at the Infrastructure for Chemical Imaging at Chalmers University of Technology, using a ToF-SIMS V instrument (ION-ToF, GmbH, Münster, Germany) equipped with a 25 keV Bismuth LMIG (Liquid metal ion gun) and a 10 keV Cs sputter gun providing high precision information on the composition of the elements, with a mass resolution m/Δm: 6000, and focus of the ion beam: 1–2 µm. The sputtered area was 650 µm × 650 µm (at 256 × 256 pixels), while the data from the central part of 450 µm × 450 µm were used for quantitative analysis to avoid possible edge effects.

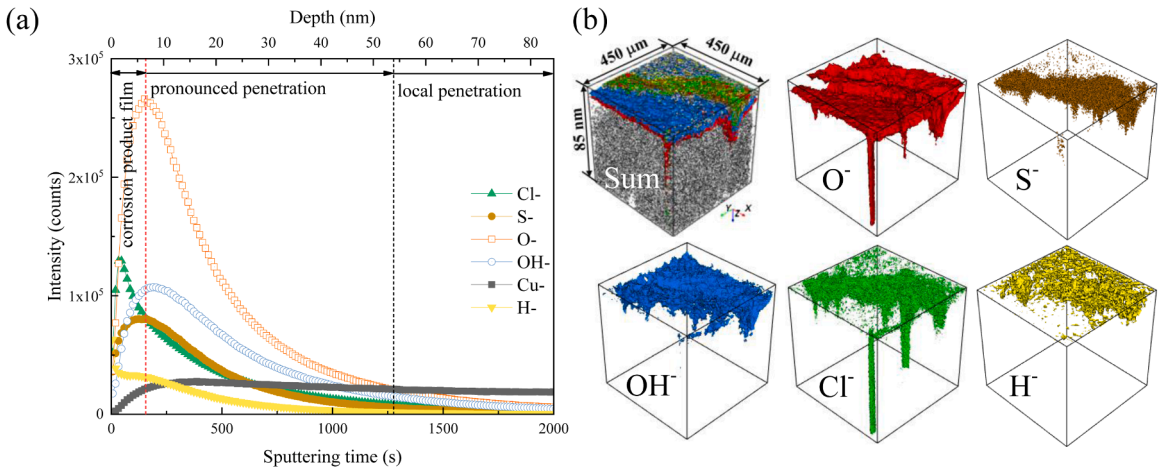

Fig. 3. (a) ToF-SIMS ion depth profiles, and (b) reconstructed ToF-SIMS 3D images of concentrated corrosive species in the volume including all the analysed areas in Fig. 2. The signal of OH^- is also included to show the presence of OH species in the corrosion products.

The signals of detected negative ions were used for plotting the depth profiles (in-depth variation of total counts over analysed area) and for construction of 2D/3D images (lateral distribution at certain depths). Both depth profile and image analyses were performed using the ION-ToF Surface Lab software (Version 6.3, ION-ToF, GmbH, Münster, Germany). The same instrument and software were used in corrosion studies as reported in previous publications [42,43]. With the setup used, the lateral resolution for imaging is ca. 0.5 μm. The mass resolution remained well above 4500–5000 with well-shaped gaussian peaks for all the elements shown in the paper, which indicates a reliable interpretation of the the ToF-SIMS data without any considerable effect of artifacts, particularly the role of topography, porosity, cracks, etc. The sputtering rate was 0.042 nm/s, determined by measuring the total depth of sputter crate using a white light interferometer (Zygo NewView7300). Note that the sputtering rate may vary slightly between the corrosion product layer and Cu matrix. However, this does not affect the discussion focusing on the penetration of the corrosive species inside the Cu matrix.

3. Results and discussion

Analysis of the ToF-SIMS data from the Cu samples provides depth profiles, revealing in-depth variations in the content of the corrosive species, and sequences of 2D images at different depths as well as 3D images of the analysed volume, showing their lateral distribution at different depth intervals. As a common practice, the signal intensity (count) vs. sputtering time is plotted in the depth profiles, and the depth value converted from the sputtering time is also added to the plots. Note that the intensity of Cu is relatively low because the ionization yield of Cu (metallic and oxidized) is much lower than that of H, S, O, and Cl due to a lower relative sensitivity factor (RSF) in ion sputtering processes. Whereas, the RSF is similar for S, H, and Cl, and somewhat higher for O, as reported in literature [35]. Ideally, the interface between the Cu metal substrate and corrosion product film is defined at the point of the rapid raise of the metal signal and the drop of the signal of corrosive species. However, it is not straightforward in this case, because some Cu grains were more corroded than others, causing uneven penetration of the corrosive species into the Cu substrate. In fact, there is no sharp boundary at the interface, therefore we define the interface at the point when the Cu signal increased to a stable level and where the signal of O or S species also started to decrease, similar to the literature report [41]. In the 2D images, the colour contrast shows the variation of the signal intensity, which indicates the difference in the concentration in a relative scale. In the 3D images, the Z-axis (depth) is not in proportion to the X and Y axes but scaled to demonstrate the changes in the distribution of corrosive species, to ease the visualization of their penetration into the Cu substrate. Note that some 3D images are included in the supplementary material.

3.1. Corrosion of Cu in simulated groundwater without Na_2S

Figs. 2 and 3 display the ToF-SIMS results from a polished sample after 9-month exposure in the simulated groundwater without Na_2S, at ambient temperature. Fig. 2 presents 2D images of Cu^-, S^-, O^-, H^- and Cl^- acquired at different depth intervals (0–21, 22–43, 44–65, and 66–87 nm) below the surface, showing lateral distribution of Cu, S, O, H and Cl in the surface and near-surface regions. The 2D images are sum frames constructed by combining individual planes obtained within certain sputtering time intervals, from which the depth ranges were calculated using the sputtering rate. To visualize the Cu grains and in some cases also the annealing twins (parallel lines), broken lines were added in the images to illustrate the grain boundaries. The sequence of the 2D images manifests the progress of the corrosion of Cu from the surface towards the interior microstructure. As seen in Fig. 2, the 2D images at all depths show some areas of higher intensity of S^-, O^-, H^-, and Cl^-, however, the intensity of Cu^- varies only slightly in these areas, indicating that the intensity variation of Cu^- is mainly originated from the different orientations of the Cu grains. Areas of lower Cu^- intensity (seen in darker contrast) are associated with the corrosion products, which could be seen only in the depth range of 0–21 nm. The correlation between the high intensity areas (seen in bright contrast) of S^-, O^-, H^-, and Cl^- indicates the joint actions of these corrosive species, and their local segregation shows nonuniform nature of the corrosion process. The corrosion products formed on the surface likely contained oxides and sulphates, probably also hydroxides and Cl-containing compounds. Thanks to the high sensitivity to detect hydrogen, the ToF-SIMS measurement revealed the distribution of H, not only in the corrosion product on the surface, but also inside the Cu microstructure (Fig. 2(d)).

Fig. 3 displays depth profiles (Fig. 3(a)) and 3D topographical images (Fig. 3(b)) for the groundwater-exposed Cu sample at a 450 μm raster size (field of view: 450 μm × 450 μm) constructed by concatenating ToF-SIMS data of concentrated corrosive species. Six signals are included in Fig. 3, the Cu^- is originated from the Cu metal and other signals represent corrosive species originating from the exposure environment. The increase of Cu^- ions was used for characterizing the matrix because the intensity of Cu^- is higher than that of Cu^{2-}, which can provide a better resolution. Based on the depth profiles of Cu^- and O^-, the thickness of the corrosion product film is estimated to be ca. 7 nm (Fig. 3(a)). This is in reasonable agreement with the average corrosion rate determined by the weight loss measurements, which include the dissolved part [34]. The

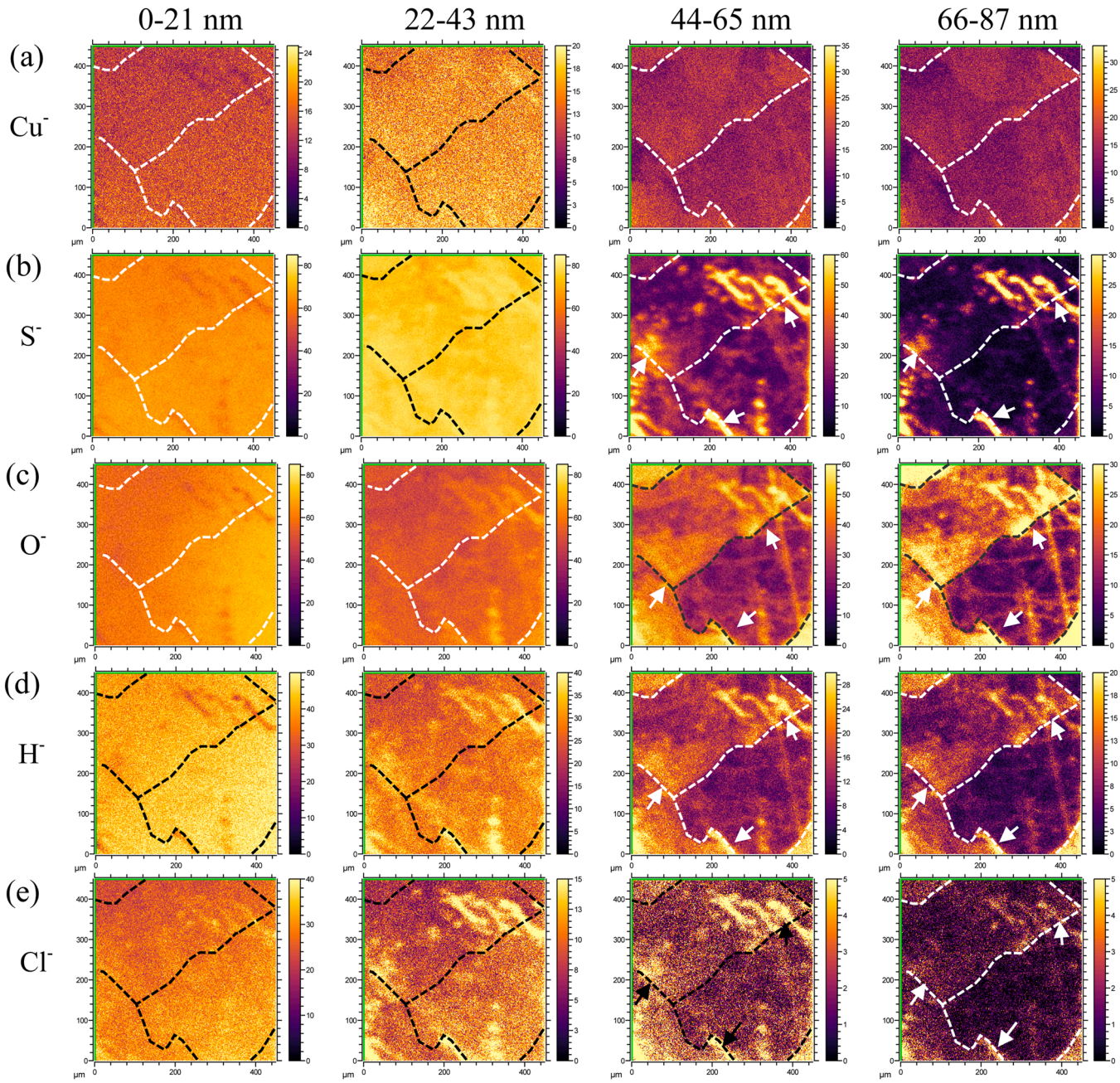

Fig. 4. Plane views by ToF-SIMS analysis at different depth intervals (0–21, 22–43, 44–65 and 66–87 nm) of a polished Cu sample after 9-month exposure in the simulated groundwater with 0.001 M Na_2S, at ambient temperature. (a) Cu^-, (b) S^-, (c) O^-, (d) H^-, and (e) Cl^-. The field of view is 450 μm × 450 μm. Arrows mark the segregation along the grain boundaries.

depth profiles show pronounced penetration of the corrosive species reaching the depth of 55 nm. Moreover, further local penetration of the corrosive species can be seen as continuously decreasing intensities with sputtering time in the logarithmic plot (supplementary Fig. S1). The pronounced penetration refers to the depth range with substantially higher contents (reflected by signal intensity) of the corrosive species distributed in a large part of the matrix, while local penetration refers to the depth range where the detected singal of the corrosive species persists and decreases with increasing depth, but still higher than the background level. The small magnitude of signal intensity beyond the background level indicates the deep penetration occurring only at some local sites. The boundary between "pronounced penetration" and "local penetration" is defined from the decline of S^-/O^- signal and the relatively stable Cu^- signal to their intersection, as shown in the depth profile plots.

The 3D images (Fig. 3(b)) visualize the corrosion product layer and local deep penetration of corrosive species (especially O and Cl) into the Cu microstructure. High level of O is seen throughout the corrosion product layer, whereas high levels of S, Cl, OH, and H are seen in some local areas. The results suggest the formation of heterogeneous corrosion products consisting of oxides/hydroxides as well as S- and Cl-containing compounds.

The sites with the deep penetration of O and Cl likely represent some grain boundaries in the microstructure. However, the width of the deep penetration channels is quite large (up to tens of μm), see Fig. 3(b), indicating the significant extent of intergranular corrosion. The ToF-SIMS results demonstrate that the Cu corrosion takes place not only through surface reactions but also through penetration of corrosive species into the Cu substrate. Without any sulfide addition, the corrosion

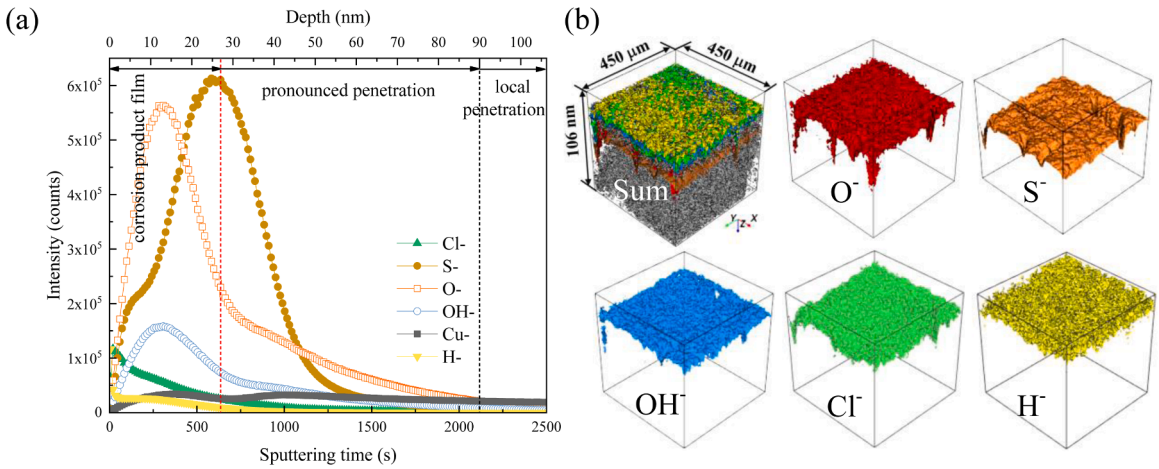

Fig. 5. (a) ToF-SIMS ion depth profiles, and (b) reconstructed ToF-SIMS 3D images of concentrated corrosive species in the volume including all the analysed areas in Fig. 4.

product layer formed on the surface is quite thin, however, the corrosion process is not uniform and local penetration of corrosive species into the Cu substrate is evident. Estimation of the penetration depth of the corrosive species, in particular S, into the Cu substrate and the implications are discussed in the summary section below.

3.2. Corrosion of Cu in simulated groundwater with 0.001 M Na_2S

Figs. 4 and 5 display the ToF-SIMS results obtained for a polished sample after 9-month exposure in the simulated groundwater with 0.001 M Na_2S, at ambient temperature. Fig. 4 presents 2D images of Cu^-, S^-, O^-, H^- and Cl^- acquired at different depth intervals below the surface, showing the lateral distribution of Cu, S, O, H and Cl in the surface and sub-surface regions, while Fig. 5 displays depth profiles and 3D images of concentrated corrosive species distributed in the entire analyzed volume. The depth intervals are chosen to be the same as those in Figs. 2 and 3 for easy comparison. It can be seen in the 2D plane views that these corrosive species, especially S and O, are present in the whole surface layer in the depth range of 0–43 nm, evidenced by the strong intensity over the whole area. Such behaviour was not detected in the absence of sulfide. With the depth exceeding 43 nm, the overall intensity for S^-, O^-, Cl^-, and H^- decreases and becomes uneven over the analysed area, indicating local segregation of the corrosive species. The distributions of S, O, Cl, and H reveal similar features, suggesting the joint action of these corrosive species. However, in the depth range of 44–87 nm, S distribution is essentially concentrated in local spots and lines (marked as arrows), whereas O distribution seems to reflect the grain orientations. The distribution of H resembles that of both O and S, and Cl level becomes very low. These findings indicate that there is some difference between these species in the local penetration and segregation in Cu microstructure. The segregation along the lines may be associated with the grain boundaries, and some of them may become preferential corrosion pathways as observed in previous studies [10, 11, 51]. These features are very different from those in the absence of sulfide, indicating its important role in the development of corrosion products and the progress of corrosion into the Cu metal.

Fig. 5 shows a thicker corrosion product film formed on the surface and also significantly enhanced penetration of the corrosive species into the Cu microstructure as compared to the case without sulfide (Fig. 3). The depth profiles in Fig. 5(a) show higher intensity of Cl^- and H^- in the outmost layer (several nm in depth), and the maximum intensity of O^- and OH^- around 12 nm. The outmost layer mainly contains oxides and hydroxides, and adsorbed species from the solution and surface contamination may also be present in this layer. The peaks of O^- and OH^- indicate the position of the oxide/hydroxide layer. Interestingly, the signal of S^- reached a maximum at the depth around 27 nm, where the intensity of O^- and OH^- decreased to a low level. Judged by the depth of maximum intensity of S^- and increased intensity of Cu^-, the thickness of the corrosion product film is estimated to be 27 nm, which is much thicker than that of the sample exposed to the groundwater without Na_2S (Fig. 3(a)). Pronounced penetration of corrosive species reached the depth of 90 nm, see Fig. 5(a), and futher local deep penetration (>106 nm) can be seen in the logarithmic plot (supplementary Fig. S2). The 3D images in Fig. 5(b) visualize the corrosion products formed on the surface, heterogenous distribution and local penetration of the corrosive species in the Cu metal. Deep local penetration is seen to follow some fast paths, seemingly along the grain boundaries, as shown in Fig. 4.

These results indicate that the corrosion product film consists of an O-rich outer layer and S-rich inner layer. The outer layer of oxide/hydroxide could be formed during the storage time after the sample was taken out from the O_2-free groundwater. The formation of a relatively thick S-rich layer on the Cu metal suggests a fast S-induced corrosion during the exposure to the O_2-free groundwater with 0.001 M Na_2S, which also leads to the significantly enhanced penetration of the corrosive species into the Cu microstructure, in particular along some fast paths. It should be mentioned that the open circuit potential value for Cu remained below - 0.8 V vs. Ag/AgCl during the entire period of exposure, indicating the reducing condition (O_2-free) of the exposure environment. Thermodynamically, this suggests the formation of copper sulfide as the main corrosion product [34]. Besides, the thickness of the corrosion product layer, ca. 27 nm, indicates that it is not a traditional passive film like that on stainless steels with the thickness of a few nm.

3.3. Effect of pre-oxidization

Figs. 6 and 7 display the ToF-SIMS results obtained for a pre-oxidized sample after 9-month exposure in the simulated groundwater with 0.001 M Na_2S, at ambient temperature. Fig. 6 presents 2D images of Cu^-, S^-, O^-, H^- and Cl^- acquired at different depth intervals from the surface, the plane views show lateral distribution of Cu, S, O, H and Cl in the surface and sub-surface regions. The pre-oxidized sample has an initial oxide film on the surface. In the surface layer (0–21 nm in depth), O is present and distributed uniformly. The O level increases towards the near-surface areas, down to the depth of 65 nm, and then decreases with increasing depth. In contrast, high level of S is present in the surface layer (0–21 nm), locally concentrated in specific grains and lines, but the level decreases with increasing depth. In the depth range of 66–87 nm, where the O intensity was lower, an increased level of S was detected again, being located in specific grains and lines. Only minor

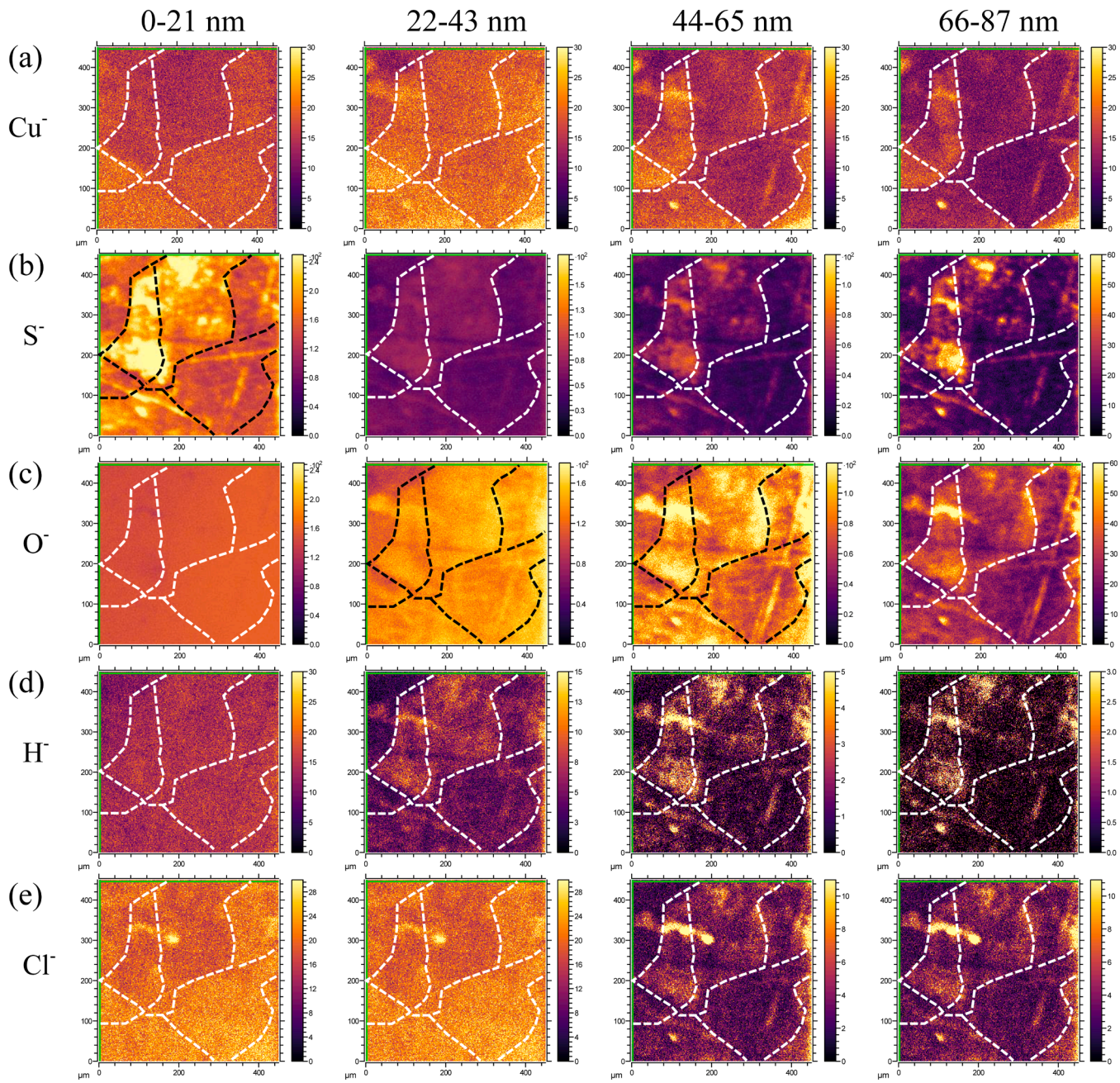

Fig. 6. Plane views by ToF-SIMS analysis at different depth intervals (0–21, 22–43, 44–65 and 66–87 nm) of a pre-oxidised Cu sample after 9-month exposure in simulated groundwater with 0.001 M Na_2S, at ambient temperature. (a) Cu^-, (b) S^-, (c) O^-, (d) H^-, and (e) Cl^-. The field of view is 450 μm × 450 μm.

levels of Cl and H were detected, being locally distributed, especially at increased depths. In this case, local penetration of the corrosive species are clearly seen in the depth range of 44–87 nm. In many sites, O and S are segregated together, and even H and Cl are seen to co-exist at some sites.

Fig. 7 displays the depth profiles of the corrosive species for a pre-oxidized sample after 9-month exposure in the simulated groundwater with 0.001 M Na_2S, at ambient temperature. The depth profiles show that the O^- peak is much higher and broader than the S^- peak. Judged by the depth of maximum S^- intensity and increased Cu^- intensity, the thickness of the corrosion product film is estimated to be ca. 25 nm, similar to that of the polished sample. Nevertheless, in this case, the depth profiles of O^- and S^- are very different from those of the polished sample (Fig. 5(a)), which has a S-dominant layer beneath the O-dominant layer. This indicates the effect of the initial oxide on the sulfide-induced corrosion process, i.e., the presence of initial oxide film reduces the sulfide-induced corrosion to some extent. However, despite of a lower intensity, the S^- peak is located slightly deeper than the O^- peak (Fig. 7). It suggests that localized S penetration can occur through the oxide film, evidenced by the similar local segregation in the surface layer (0–21 nm in depth) and inside the Cu substrate (66–87 nm in depth), see Fig. 6(b). The heterogenous corrosion products, the pronounced penetration of the corrosive species into the Cu substrate down to the depth of 147 nm, and further local penetration can be viewed in the 3D images and the log plot of depth profiles (supplementary Fig. S3). These results indicate that the exposure of the pre-oxidized sample to the anoxic groundwater with 0.001 M Na_2S results in both the formation of O- and S-rich compounds on the surface and also penetration of the corrosive species into the Cu microstructure, despite the presence of an initial oxide film on the surface. The corrosive species seem to have some

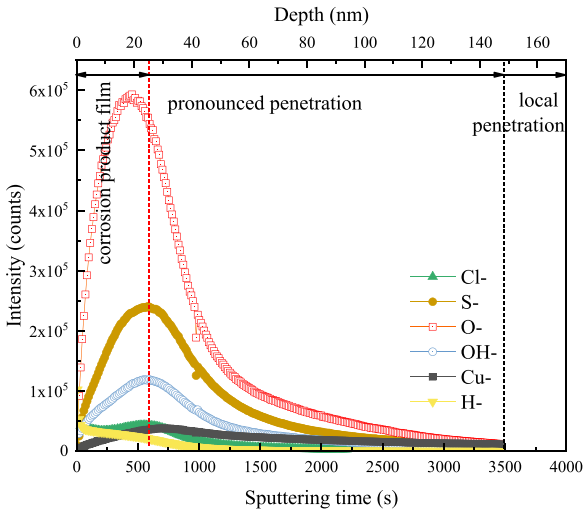

Fig. 7. ToF-SIMS ion depth profiles of concentrated corrosive species in the volume including all the analysed areas in Fig. 6.

joint actions that promote their penetration into the Cu microstructure.

3.4. Effect of elevated exposure temperature of 60 °C

Figs. 8 and 9 display 2D images obtained from two pre-oxidized samples after 4-month exposure in the simulated groundwater with 0.001 M Na_2S, one at ambient temperature (22 °C), and another at 60 °C. The total sputtering time is 2500 s for the sample exposed at ambient temperature and 12000 s for the one exposed at 60 °C, respectively. The latter was much longer because of a much deeper penetration of the corrosive species. In Fig. 8(a), the contrast in Cu^- intensity reflects the different crystallographic orientations of the grains (with different atomic packing densities). The S^- and O^- signals are strong and quite uniform in the surface layer (0–25 nm in depth), and decrease in the overall intensity with increasing depth. Beyond 25 nm, S^- and O^- signals show localized high intensity, indicating their joint penetration into the Cu microstructure. The H^- and Cl^- signals, although relatively weak, were also detected within the Cu metal, mostly appearing as small spots located along and in the vicinity of the grain boundaries. These small spots are likely the trapping sites of H and other corrosive species. Local deep penetration of the corrosive species, seemingly along grain boundaries, can be viewed in the log plot of depth profiles and the 3D images (supplementary Fig. S4(a) and (c)).

For the sample exposed to Na_2S-added groundwater at 60 °C, because of a thicker corrosion product film and deeper penetration of corrosive species, larger depth intervals are used for constructing 2D images, see Fig. 9. The contrast in Cu^- intensity reveals high-angle boundaries (added broken lines), which are likely high-angle grain boundaries and twins. The S^- images show a high level of S uniformly distributed down to the depth of 250 nm, while it is concentrated along the lines at greater depths, consistent with the Cu^- images. The O^- intensity from the surface down to 250 nm is much lower than for S^-, but consistent trends are seen for S^- and O^- images obtained at greater depths. In the S^- and O^- images for the depth range of 376–500 nm, lines with relatively high signal intensity are seen inside large grains, which are likely associated with the grinding scratches (with residual strain and concentrated dislocations) on the sample. Overall, the S^- signal has the highest intensity in the whole analysed area down to the depth of 375 nm, suggesting that S is the dominant corrosive species in the corrosion product film. Local enrichment of the corrosive species is seen in the depth range of 250–375 nm, and their segregation along the lines and at many spots was detected in the depth range of 376–500 nm. Interestingly, the spots appear as being connected along certain lines, which may be associated with a large extent of segregation along the grain and sub-grain boundaries. The heterogenous corrosion products on the surface and local deep penetration of the corrosive species can be viewed in the log plot of depth profiles and the 3D images (supplementary Fig. S4(b) and (d)).

For comparison, the depth profiles for the two samples are plotted in Fig. 10. In both cases, S^- has a higher intensity than O^-, and the S^- peak is broader than the O^- peak. Obviously, the corrosion product film is much thicker and the penetration of the corrosive species is much deeper for the sample exposed at 60 ℃ than the one exposed at ambient temperature. Judged from the O^-, S^-, and Cu^- profiles, the thickness of the corrosion product film is estimated to be ca. 25 nm for the sample exposed at ambient temperature, while it is around 170 nm for the sample exposed at 60 °C. It is striking that the high intensity of S^- extends deep into the Cu substrate when exposed at 60 °C. Pronounced penetration of S reached the depth of 440 nm (Fig. 10(b)), while the local penetration along grain boundaries is likely much deeper. Clearly, the sulfide-induced corrosion of Cu in the anoxic groundwater is greatly accelerated by increasing the exposure temperature to 60 °C, and the ingress of the corrosive species, especially S, is largely promoted by the increased temperature.

4. Overall discussion and implications of the results

In this work, after the exposure runs, the Cu samples were stored in desiccators for a long time and then in air for many days before the ToF-SIMS analysis. During the storage in air, conversion of some part of sulfides to oxides is possible due to oxidation. Meanwhile, surface adsorption and contamination may occur during this period leading to modification of the outermost layer (a few nm thick). Moreover, due to the large Cu grains, up to a few hundreds of μm in size, the analysed area (450 μm × 450 μm) may only include a small number of grains, so caution should be taken in quantitative comparison between the samples. Furthermore, the sample surface area selected for ToF-SIMS analyses were relatively smooth, without visible porosity and cracks. The morphology of the corrosion scale is shown in Fig. S5. The results show detectable levels of the corrosive species in all cases, and some other areas may have even higher levels. The 2D images and linear plots of the depth profiles reveal pronounced penetration of the corrosive species, while the depth of local penetration is much deeper in some cases, judged by the logarithmic plots (highlighting small changes). To determine the local penetration depth requires long sputtering times until reaching the depth where the corrosive species is reduced to the background level. Since H atoms are highly mobile even at ambient temperature, part of atomic H entering into the Cu during the exposure in the groundwater may have egressed from the sample during the storage time before the ToF-SIMS analysis. Thus, the detected H is only the trapped part. Accurate quantitative measurement of H requires freezing the sample before the measurement, and Nano-SIMS with nm lateral resolution is needed to resolve H segregation along grain boundaries. The ToF-SIMS data presented here are given in counts/intensity, showing the variations on a relative scale. Nevertheless, the ToF-SIMS results, showing both the depth profiles including in-depth variations and penetration of the corrosive species into the Cu substrate, and the 2D/3D images showing uneven distribution and local segregation of the corrosive species within the Cu microstructure, provide valuable information about the corrosion processes occurring not only on the Cu surface, but also inside the Cu microstructure. This information is often missing in corrosion studies.

The ToF-SIMS depth profiles of the corrosive species often show a peak followed by slow decay of the signal intensity with sputtering time. The high levels of S and O, together with a lower level of Cu, is associated with a S- and O-rich corrosion product film formed on the surface, while the slow decay of the corrosive species indicates their penetration into the Cu substrate. Deep penetration is seen to occur along some fast paths, e.g., grain boundaries, Figs. 2 and 4. The 2D images clearly show that locally concentrated S, O, H, and Cl often overlap in the same areas

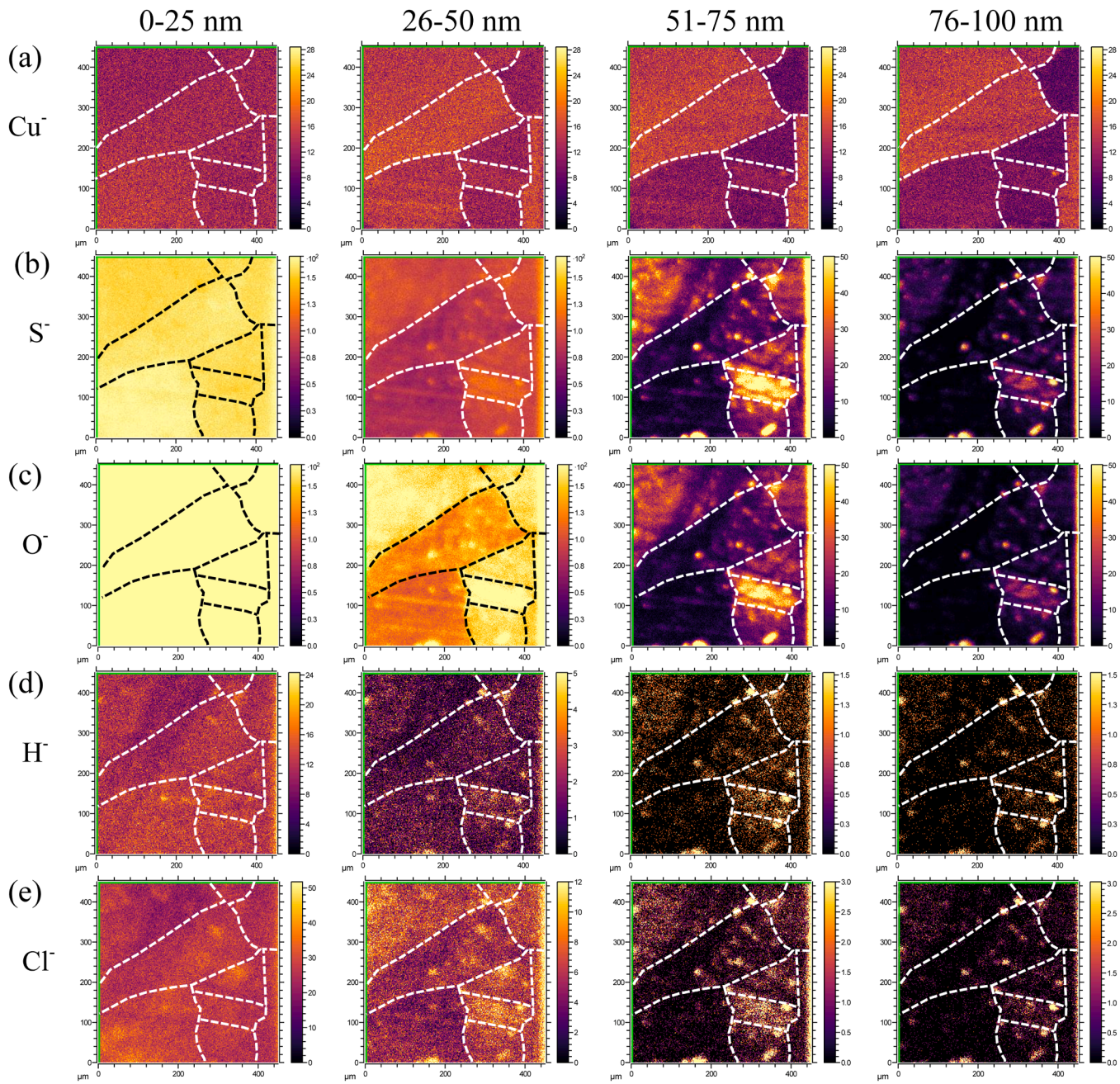

Fig. 8. Plane views by ToF-SIMS analysis at different depths (0–25, 26–50, 51–75, and 76–100 nm) of a pre-oxidised Cu sample after 4-month exposure in the simulated groundwater with 0.001 M Na_2S, at ambient temperature. (a) Cu^-, (b) S^-, (c) O^-, (d) H^-, and (e) Cl^-. The field of view is 450 μm × 450 μm.

or sites, suggesting their joint action in the corrosion process. An initial oxide film, either formed due to exposure in air or during pre-oxidation, was present on the surface before the exposure to the groundwater. During the long-term exposure to the simulated anoxic groundwater, the initial oxide film does not seem to prevent the transport of corrosive species and further corrosion of the metal. The results in Figs. 2 and 3 show that, without Na_2S addition, a thin oxide/hydroxide layer remained on the surface after the exposure, and local penetration of S, O, H, and Cl into Cu substrate occurred, seemingly along grain boundaries. In this case, the S originates from SO_4^{2-}, and Cl from Cl^- ions, both of which were involved in the corrosion process. In the presence of Na_2S (0.001 M), the corrosion was significantly accelerated, evidenced by a thicker corrosion product film formed on the surface and the enhanced penetration of the corrosive species, especially S, and deep local penetration into the Cu substrate (Figs. 4 and 5). The correlation between S^- and CuS^- in the depth profiles (Fig. S6) suggests that the S-compound in the S-rich corrosion products formed on the surface is most likely Cu sulfide [34].

Comparison of the results from the polished and pre-oxidized samples shows the effect of the pre-oxidation. On the polished sample, the corrosion product film consists of an O-rich outer layer and a S-rich inner layer (Fig. 5). Whereas, on the pre-oxidized sample, the corrosion product film contains mixed O- and S-compounds (oxides and sulfides), in which the O-compounds are dominant (Fig. 7). In both cases, significant penetration and local segregation of S, O, H, and Cl in the Cu microstructure occurred (Figs. 4 and 6). These results indicate that the initial oxide film formed during the pre-oxidation did not act as a dense barrier to impede the sulfide-induced corrosion, and S-species could easily penetrate the initial oxide film. Probably, the initial oxide film is defective or soluble in the groundwater, which allows easy penetration

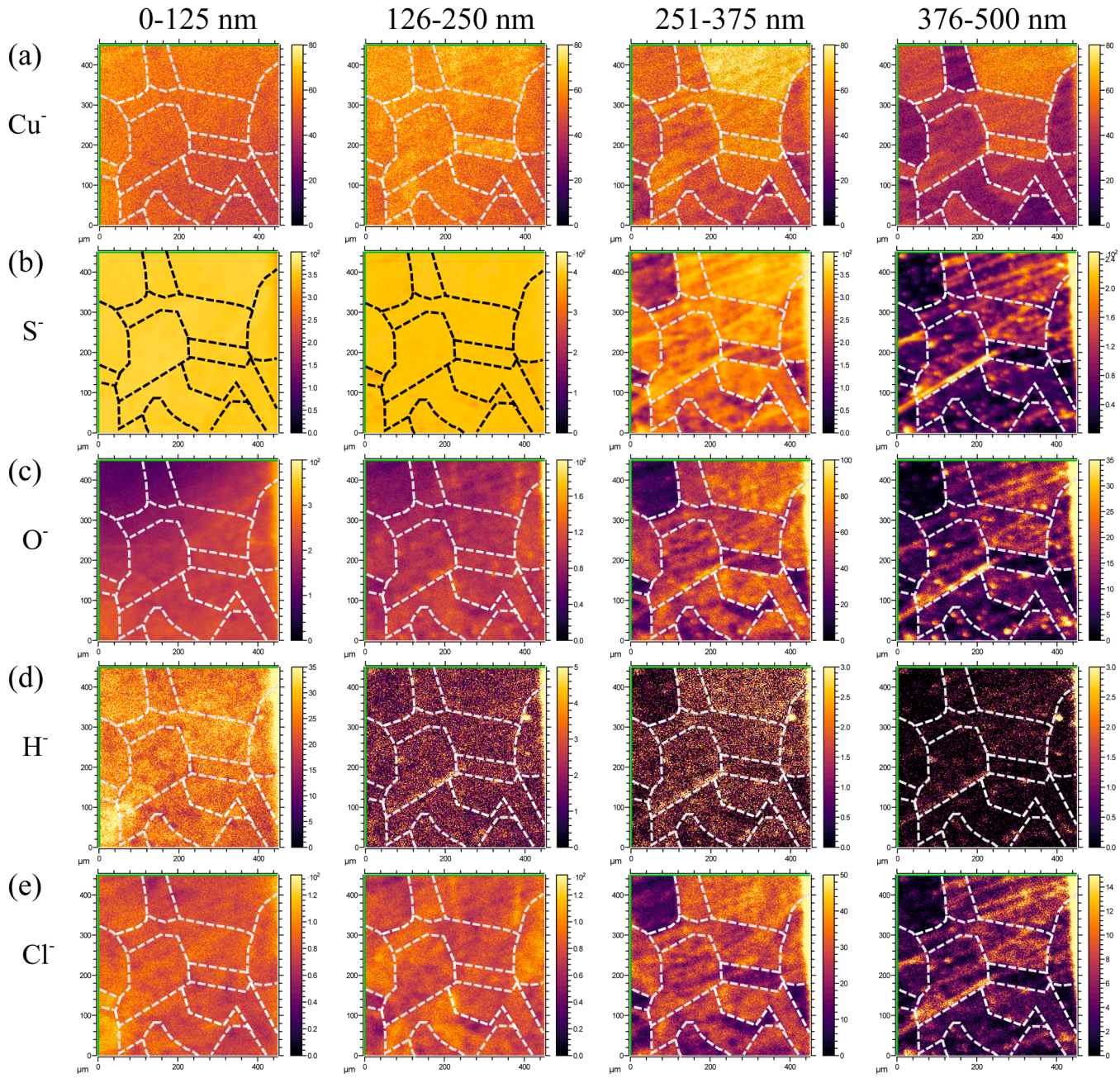

Fig. 9. Plane views by ToF-SIMS analysis at different depths (0–125, 126–250, 251–375, and 375–500 nm) of a pre-oxidised Cu sample after 4-month exposure in the simulated groundwater with 0.001 M Na_2S, at 60 ºC. (a) Cu^-, (b) S^-, (c) O^-, (d) H^-, and (e) Cl^-. The field of view is 450 μm × 450 μm.

of the S-species. In fact, the presence of a discontinuous oxide film, especially when containing oxide particles at the grain boundaries, facilitates hydrogen trapping [11]. Comparison of the results from the exposure at ambient temperature and at 60 °C show clearly that the increased temperature of 60 °C has a pronounced effect by accelerating the sulfide-induced corrosion, and the role of S-compounds is more enhanced than that of O-compounds. The thickness of the corrosion product film increased several times and the film became dominated by S-compounds (Fig. 10). Penetration of S and O into the Cu substrate was greatly promoted, and the local segregation of S, O, and Cl occurred more frequently and to a larger extent than at ambient temperature, appearing as continuous lines instead of discrete spots (Figs. 7 and 8). The local distribution of H is probably similar, but this needs to be confirmed by further Nano-SIMS analysis. The temperature effect on the penetration of S, O, and Cl into the Cu substrate can clearly be seen from the comparison of depth profiles in Fig. 11.

Thermodynamics and kinetics of Cu corrosion in pure water and simulated groundwater have been studied extensively, with respect to the deep geological disposal of nuclear waste [6,8]. Under anoxic condition, in the presence of sulfide, surface Cu-oxides will be transformed into Cu-sulfides [16,17]. DFT calculations of simple model systems suggest possible dissociation of H_2O and sulfide species and adsorption of O, H, and S on the Cu surface [18,19,46–49]. It has been claimed that ingress of H and S into the Cu lattice is not energetically favourable [32], based on the calculations showing possible formation of H_2 is some cases [47,48,50]. However, in real disposal system, high levels of Cl^- and SO_4^{2-} and also of sulfide species are present in the groundwater. Moreover, there are various types of defects on the Cu surface and inside the microstructure including dislocations, grain boundaries and voids. The ToF-SIMS results from this work demonstrate that, during exposure of

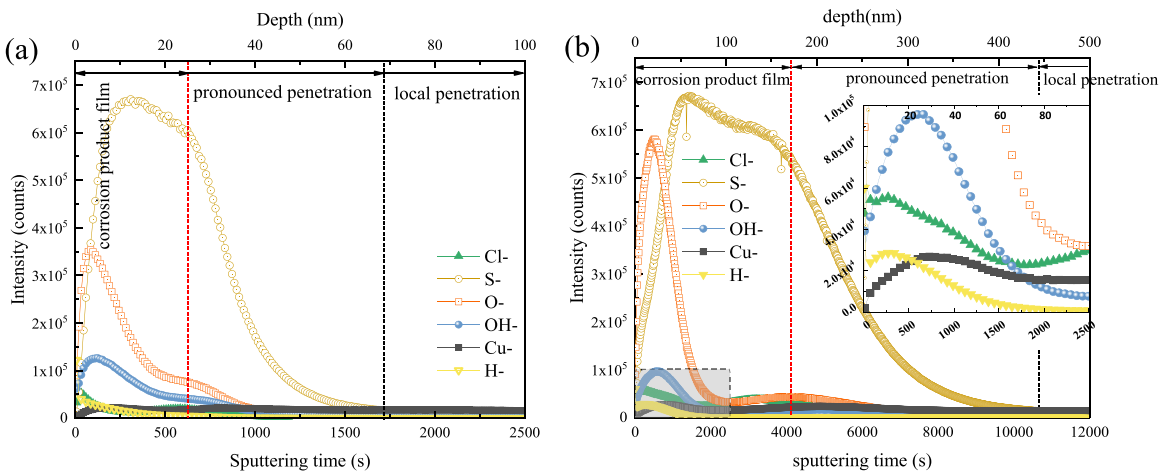

Fig. 10. ToF-SIMS ion depth profiles for the pre-oxidized Cu samples after 4-month exposure in the simulated groundwater with 0.001 M Na_2S, (a) at ambient temperature, and (b) at 60 ºC. Note the depth scale in (b) is 5 times of that in (a).

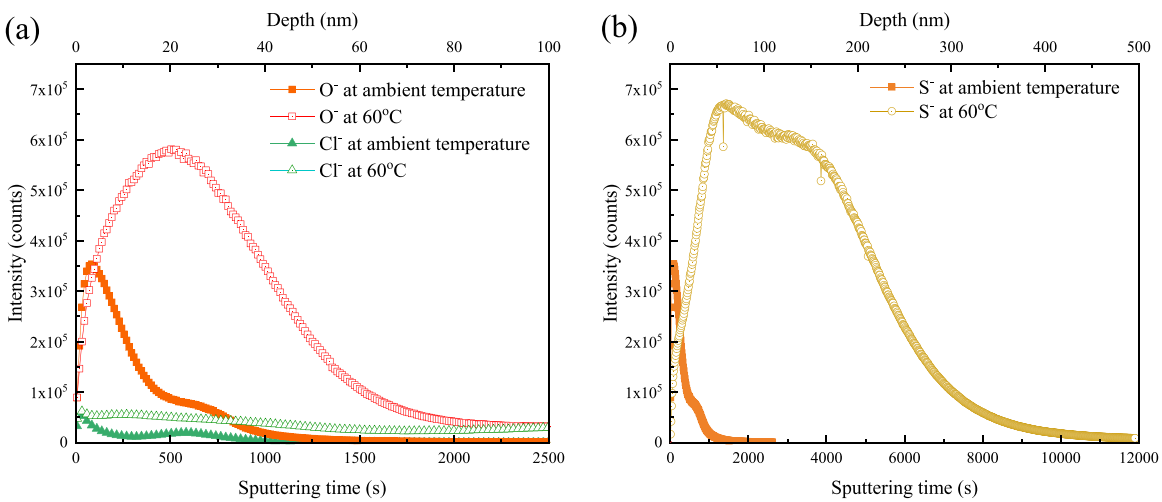

Fig. 11. ToF-SIMS ion depth profiles of (a) O^- and Cl^-, and (b) S^- on the samples after 4-month exposure in the simulated groundwater with 0.001 M Na_2S, at ambient temperature and 60 °C, respectively.

Cu samples to the groundwater, in addition to the formation of complex corrosion products on the surface, significant penetration of S, H occurs in the Cu microstructure, often observed with joint penetration of O and Cl. This local penetration of corrosion stimulating species down to the depth of several hundred nanometres along some fast paths occurs, even without added sulfide. Such local penetration suggests a severe underestimation of the corrosion risk of Cu when only considering the homogeneous corrosion processes. Furthermore, such penetration is enhanced by the sulfide addition. The elevated temperature of 60 °C greatly accelerates the corrosion on the surface and the penetration of corrosive species into the Cu substrate. Fig. 12 shows an illustration of the corrosion processes including the penetration of the S, O, H and Cl into the Cu microstructure.

The ToF-SIMS results provide clear evidence for the pronounced penetration of S, O, H and Cl into the Cu microstructure, which is heterogenous and seems to be related to the grain orientations. The grain-orientation effect on the corrosion process has also been observed by other measurements [34]. Deep penetration occurs via some fast paths, likely along some grain boundaries. These new findings provide reasonable explanations for the observations of sulfide-induced SCC and intergranular corrosion of Cu in similar environments [10,11,51]. The most striking observation is the pronounced penetration of S into Cu which is enhanced by the sulfide addition and greatly promoted by the elevated temperature of 60 °C. Based on the ToF-SIMS ion depth profiles and the 2D maps of the distribution of the corrosive species (in the grains and along the grain boundaries), the depth of pronounced penetration can be determined for the different samples. As can be seen in the log plots of the depth profiles, the depth of local penetration along grain boundaries exceeds the depth of termination of the ion sputtering. Taking the Cu sample after 4-month exposure to the Na_2S-added groundwater at 60 °C as an example, the results show that the pronounced S penetration (involving diffusion both within the grains and along the grain boundaries) reached the depth of 440 nm, whereas the depth of local penetration (along the grain boundaries) is beyond 500 nm. Assuming linear extrapolation it follows that the overall penetration rate of S is 1.32 μm/year and the rate of S penetration along grain boundaries is more than 1.5 μm/year. These rates can be used to estimate the time needed for S to penetrate the Cu metal under service conditions. Accordingly, it takes ca. 38 years and 38000 years for S to penetrate 50 μm and 5 cm thick Cu, respectively. Moreover, it takes less than ca. 33 and 33000 years for S to diffuse 50 μm and 5 cm, respectively, along the grain boundaries. These values can be compared with an SKB report compiling data of diffusion in Cu [58]. According to Figs. 3–5 in ref. 58, at 60 °C, it takes less than 1000 years for S to diffuse 5 cm in grain boundaries. In our ToF-SIMS measurements, the local S penetration along the grain boundaries could be much deeper than the

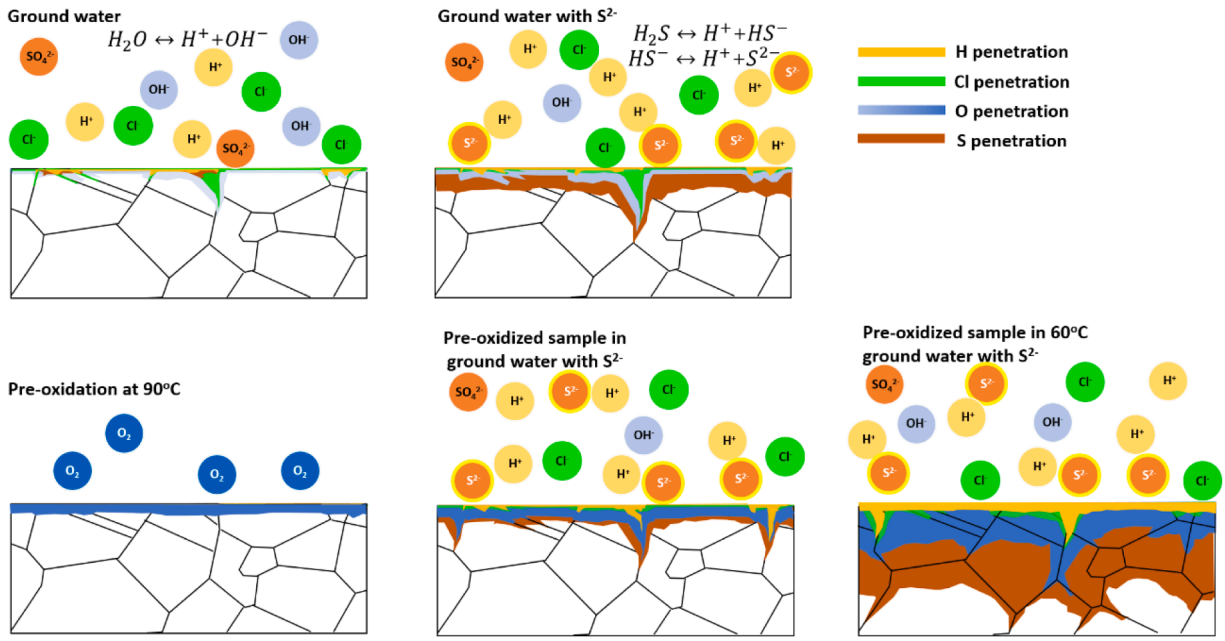

Fig. 12. Illustration of penetration of corrosive species into the Cu microstructure under different exposure conditions.

depth of termination of the ion sputtering, therefore our extrapolated results are in general agreement with the above calculation using the reported diffusion data [58]. The ToF-SIMS results demonstrate that the S penetration into the Cu microstructure and the local penetration along grain boundaries are indeed very fast under the experimental conditions.

To understand the mechanism of the internal corrosion and penetration of corrosive species inside the microstructure requires detailed knowledge at atomistic scale, typically acquired by DFT calculations. The joint actions of S and H, together with O and Cl, may have some synergistic effect on the corrosion process, which has not been addressed by DFT, although hydrogen trapping and sorption capacity was calculated for vacancy, void and grain boundaries in Cu [52–54]. A theoretical study of diffusion of dissociation products suggests that OH in a grain boundary of Cu quickly dissociates leading to fast diffusion of O and H atoms along the grain boundary [55]. Moreover, DFT calculations show that S and P tend to segregate and thus accumulate at a certain type of grain boundary in Cu [56]. In a study of impurity effects on the grain boundary cohesion in Cu, it has been found that a strong segregation of S can reduce the work (energy) of grain boundary separation below the work of dislocation emission, thus embrittling Cu, which is in agreement with experimental observations [57].

Our new findings have important implications regarding the risk for sulfide-induced SCC and embrittlement of the Cu canister. A comprehensive understanding of the corrosion mechanism is needed to provide a solid scientific basis for the risk assessment of the Cu canister in the final disposal of nuclear waste. This should include the local strain formation in the near surface region and in the bulk microstructure of the Cu, as reported previously [19]. Thus, it is crucial to take into account the internal corrosion processes occurring underneath the corrosion product film and the damage of the Cu microstructure caused by the ingress of the corrosive species in the risk assessment of Cu canister [19]. It should be mentioned that the additional radiation effect on the corrosion process caused by highly radioactive spent fuel is not included herein and needs to be considered in future studies.

5. Conclusions

The ToF-SIMS measurements of copper samples after exposures for several months to the simulated O_2-free groundwater with and without sulfide addition provide depth profiles of concentrated corrosive species, 2D images of lateral distribution of the corrosive species at different depth intervals, and 3D images showing deep local penetration along some fast paths. Based on the results, the following conclusions can be drawn:

- During the exposure, in addition to the formation of a corrosion product film on the Cu surface, pronounced penetration of the corrosive species, H, S, O, and Cl, into Cu metal occurs in the near surface region, and deep local penetration proceeds at certain fast paths, most likely along some grain boundaries. This happens even in the absence of sulfide addition.

- The corrosion process of Cu is heterogenous and influenced by the crystallographic orientation of the Cu grains. The corrosion products formed on the surface consist mainly of O- and S-compounds and also of minor Cl-components. The corrosive species, H, S, O, and Cl often segregate together and likely exhibit joint actions, resulting in internal corrosion.

- The corrosion processes, both the formation of the corrosion product film on the surface and penetration of the corrosive species inside the Cu metal, are significantly enhanced by the sulfide addition (Na_2S) at a concentration of 0.001 M, which results in essentially S-rich corrosion products. The initial oxide film formed by pre-oxidation does not act as an effective barrier to the sulfide-induced corrosion.

- The elevated temperature of 60 °C during the exposure greatly accelerates the sulfide-induced corrosion, leading to a several times increase in the thickness of the corrosion product film and the deep penetration of the corrosive species. After four months S reaches 440 nm into the Cu substrate and more than 500 nm along local fast paths.

- The evidence of penetration of the corrosive species, H, S, O, and Cl, especially their deep local penetration into the Cu microstructure, implies the risk for embrittlement and crack initiation in the Cu material. This demonstrates the need for thorough evaluation of sulfide-induced complex forms of Cu corrosion in the risk assessment of Cu canister.

CRediT authorship contribution statement

Xiaoqi Yue: Data curation, Formal analysis, Investigation, Methodology, Writing - original draft. **Per Malmberg:** Data curation, Formal analysis, Methodology, Writing - original draft. **Elisa Isotahdon, Vilma Ratia-Hanby, Elina Huttunen-Saarivirta:** Sample preparation and

immersion tests, Writing - review & editing. **Christofer Leygraf:** Investigation, Visualization, Writing - review & editing. **Jinshan Pan:** Conceptualization, Data curation, Investigation, Methodology, Writing - original draft, Supervision.

Declaration of Competing Interest

The authors declare that they have no known competing financial interests or personal relationships that could have appeared to influence the work reported in this paper.

Data Availability

Data will be made available on request.

Acknowledgement

The financial supports from NKS (Contract AFT/NKS-R(21)127/2) and Swedish Research Council (Vetenskapsrådet, project no. 2021-04157) are greatly acknowledged.

Appendix A. Supporting information

Supplementary data associated with this article can be found in the online version at doi:10.1016/j.corsci.2022.110833.

References

[1] Saanio, T.; Ikonen, A.; Keto, P.; Kirkkomäki, T.; Kukkola, T.; Nieminen, J.; Raiko, H. Design of the Disposal Facility 2012; POSIVA-WR-13–17; Posiva, Finland, 2013.
[2] Saanio, T.; Ikonen, A.; Keto, P.; Kirkkomäki, T.; Kukkola, T.; Nieminen, J.; Raiko, H. Design of the Disposal Facility 2012; POSIVA-WR-13–17; Posiva, Finland, 2013.
[3] E. Huttunen-Saarivirta, P. Rajala, M. Bomberg, L. Carpén, Corrosion of copper in oxygen-deficient groundwater with and without deep bedrock micro-organisms: characterisation of microbial communities and surface processes, Appl. Surf. Sci. 396 (2017) 1044, https://doi.org/10.1016/j.apsusc.2016.11.086.
[4] L. Carpen, P. Rajala, M. Bomberg, Corrosion of copper in anoxic ground water in the presence of SRB, Corros. Sci. Technol. 17 (2018) 147, https://doi.org/10.14773/CST.2018.17.4.147.
[5] E. Huttunen-Saarivirta, E. Ghanbari, F. Mao, P. Rajala, L. Carpén, D.D. Macdonald, Kinetic properties of the passive film on copper in the presence of sulfate-reducing bacteria, J. Electrochem. Soc. 165 (2018) C450, https://doi.org/10.1149/2.007189jes.
[6] D.S. Hall, M. Behazin, W. Jeffrey Binns, P.G. Keech, An evaluation of corrosion processes affecting copper-coated nuclear waste containers in a deep geological repository, Prog. Mater. Sci. 118 (2021), 100766, https://doi.org/10.1016/j.pmatsci.2020.100766.
[7] F. King, M. Kolář, I. Puigdomenech, P. Pitkänen, C. Lilja, Modeling microbial sulfate reduction and the consequences for corrosion of copper canisters, Mater. Corros. 72 (2021) 339, https://doi.org/10.1002/maco.202011770.
[8] F. King, C. Lilja, K. Pedersen, P. Pitkänen, M. Vähänen, An Update of the State-of-the-art Report on the Corrosion of Copper under Expected Conditions in A Deep Geologic Repository, SKB-10-67, Swedish Nuclear Fuel and Waste Management Co., Sweden, 2010.
[9] C. Padovani, F. King, C. Lilja, D. Féron, S. Necib, D. Crusset, V. Deydier, N. Diomidis, R. Gaggiano, T. Ahn, P.G. Keech, D.D. Macdonald, H. Asano, N. Smart, D.S. Hall, H. Hänninen, D. Engelberg, J.J. Noël, D.W. Shoesmith, The corrosion behaviour of candidate container materials for the disposal of high-level waste and spent fuel – a summary of the state of the art and opportunities for synergies in future R&D, Corros. Eng. Sci. Technol. 52 (2017) 227, https://doi.org/10.1080/1478422X.2017.1356973.
[10] R. Becker, J. Öijerholm, Slow Strain Rate Testing of Copper in Sulfide Rich Chloride Containing Deoxygenated Water at 90 °C, SSM 2017:02, Swedish Radiation Authority, Sweden, 2017.
[11] A. Forsström, R. Becker, H. Hänninen, Y. Yagodzinskyy, M. Heikkilä, Sulphide-induced stress corrosion cracking and hydrogen absorption of copper in deoxygenated water at 90°C, Mater. Corros. 72 (2021) 317, https://doi.org/10.1002/maco.202011695.
[12] C.M. Lousada, I.L. Soroka, Y. Yagodzinskyy, N.V. Tarakina, O. Todoshchenko, H. Hänninen, P.A. Korzhavyi, M. Jonsson, Gamma radiation induces hydrogen absorption by copper in water, Sci. Rep. 6 (2016) 24234, https://doi.org/10.1038/srep24234.
[13] I. Soroka, N. Chae, M. Jonsson, On the mechanism of γ-radiation-induced corrosion of copper in water, Corros. Sci. 182 (2021), 109279, https://doi.org/10.1016/j.corsci.2021.109279.
[14] J. Chen, Z. Qin, D.W. Shoesmith, Kinetics of corrosion film growth on copper in neutral chloride solutions containing small concentrations of sulfide, J. Electrochem. Soc. 157 (2010) C338, https://doi.org/10.1149/1.3478570.
[15] J. Chen, Z. Qin, T. Martino, M. Guo, D.W. Shoesmith, Copper transport and sulphide sequestration during copper corrosion in anaerobic aqueous sulphide solutions, Corros. Sci. 131 (2018) 245, https://doi.org/10.1016/j.corsci.2017.11.025.
[16] J.M. Smith, J.C. Wren, M. Odziemkowski, D.W. Shoesmith, The electrochemical response of preoxidized copper in aqueous sulfide solutions, J. Electrochem. Soc. 154 (2007) C431, https://doi.org/10.1149/1.2745647.
[17] H.M. Hollmark, P.G. Keech, J.R. Vegelius, L. Werme, L.-C. Duda, X-Ray absorption spectroscopy of electrochemically oxidized Cu exposed to Na_2S, Corros. Sci. 54 (2012) 85, https://doi.org/10.1016/j.corsci.2011.09.001.
[18] C.M. Lousada, A.J. Johansson, P.A. Korzhavyi, Molecular and dissociative adsorption of water and hydrogen sulfide at perfect and defective Cu(110) surfaces, Phys. Chem. Chem. Phys. 19 (2017) 8111.
[19] F. Zhang, C. Örnek, M. Liu, T. Müller, U. Lienert, V. Ratia-Hanby, L. Carpén, E. Isotahdon, J. Pan, Corrosion-induced microstructure degradation of copper in sulfide-containing simulated anoxic groundwater studied by synchrotron high-energy X-ray diffraction and ab-initio density functional theory calculation, Corros. Sci. 184 (2021), 109390.
[20] J.B. Condon, T. Schober, Hydrogen bubbles in metals, J. Nucl. Mater. 207 (1993) 1–24, https://doi.org/10.1016/0022-3115(93)90244-S.
[21] T.G. Nieh, W.D. Nix, The formation of water vapor bubbles in copper and their effect on intergranular creep fracture, Acta Metall. 28 (1980) 557, https://doi.org/10.1016/0001-6160(80)90122-4.
[22] S. Nakahara, Microscopic mechanism of the hydrogen effect on the ductility of electroless copper, Acta Metall. 36 (1988) 1669, https://doi.org/10.1016/0001-6160(88)90234-9.
[23] Y. Okinaka, H.K. Straschil, The effect of inclusions on the ductility of electroless copper deposits, J. Electrochem. Soc. 133 (1986) 2608, https://doi.org/10.1149/1.2108489.
[24] M.G. Ganchenkova, Y.N. Yagodzinskyy, V.A. Borodin, H. Hänninen, Effects of Hydrogen and Impurities on Void Nucleation in Copper: Simulation Point of View, Philos. Mag. 94 (31) (2014) 3522–3548, https://doi.org/10.1080/14786435.2014.962642.
[25] Y. Yagodzinskyy, E. Malitckii, F. Tuomisto, H. Hänninen, Hydrogen-induced strain localisation in oxygen-free copper in the initial stage of plastic deformation, Philos. Mag. 98 (9) (2018) 727–740, https://doi.org/10.1080/14786435.2017.1417647.
[26] A. Forsström, S. Bossuyt, Y. Yagodzinskyy, K. Tsuzaki, H. Hänninen, Strain localization in copper canister FSW welds for spent nuclear fuel disposal, J. Nucl. Mater. 523 (2019) 347–359, https://doi.org/10.1016/j.jnucmat.2019.06.024.
[27] Y. Yagodzinskyy, E. Malitckii, T. Saukkonen, H. Hänninen, Hydrogen-enhanced creep and cracking of oxygen-free phosphorus-doped copper, Scr. Mater. 67 (12) (2012) 931–934, https://doi.org/10.1016/j.scriptamat.2012.08.018.
[28] Å. Martinsson, R. Sandström, C. Lilja, Hydrogen in Oxygen-Free, Phosphorus-Doped Copper: Charging Techniques, Hydrogen Contents and Modelling of Hydrogen Diffusion and Depth Profile, SKB-TR-13-09, Swedish Nuclear Fuel and Waste Management Co, Sweden, 2013.
[29] Å. Martinsson, R. Sandström, Hydrogen depth profile in phosphorus-doped, oxygen-free copper after cathodic charging, J. Mater. Sci. 47 (2012) 6768, https://doi.org/10.1007/s10853-012-6592-y.
[30] N. Taniguchi, M. Kawasaki, Influence of sulfide concentration on the corrosion behavior of pure copper in synthetic seawater, J. Nucl. Mater. 379 (2008) 154.
[31] Supplementary Information on Canister Integrity Issues, SKB TR-19–15, Swedish Nuclear Fuel and Waste Management Co, 2019.
[32] A. Hedin, J. Johansson, F. King, Comment on "corrosion-induced microstructure degradation of copper in sulfide-containing simulated anoxic groundwater studied by synchrotron high-energy X-ray diffraction and Ab-initio density functional theory calculation, Corros. Sci. 199 (2022), 110182, https://doi.org/10.1016/j.corsci.2022.110182.
[33] J. Pan, C. Örnek, U. Lienert, M. Liu, T. Müller, F. Zhang, V. Ratia-Hanby, L. Carpén, E. Isotahdon, Reply to comment on "corrosion-induced microstructure degradation of copper in sulfide-containing simulated anoxic groundwater studied by synchrotron high-energy X-ray diffraction and Ab-initio density functional theory calculation, Corros. Sci. 199 (2022), 110183, https://doi.org/10.1016/j.corsci.2022.110183.
[34] E. Isotahdon, V. Ratia-Hanby, E. Huttunen-Saarivirta, X. Yue, J. Pan, Corrosion of copper in sulphide containing environment: the role and properties of sulphide films – Annual report 2021, NKS-460, Nordic Nuclear Safety Research NKS, 2022. https://www.nks.org/en/nks_reports/view_document.htm?
[35] D.S. Mcphail, Applications of secondary ion mass spectrometry (SIMS) in materials science, J. Mater. Sci. 41 (2006) 873.
[36] John C. Vickerman, David Briggs (Eds.), ToF-SIMS: Materials Analysis by Mass Spectrometry, 2nd ed., SurfaceSpectra Ltd., 2012.
[37] T. Wirtz, P. Philipp, J.-N. Audinot, D. Dowsett, S. Eswara, High-resolution high-sensitivity elemental imaging by secondary ion mass spectrometry: from traditional 2D and 3D imaging to correlative microscopy, Nanotechnology 26 (2015), 434001.
[38] J. Ekar, P. Panjan, S. Drev, J. Kovač, ToF-SIMS depth profiling of metal, metal oxide, and alloy multilayers in atmospheres of H_2, C_2H_2, CO, and O_2, J. Am. Soc. Mass Spectrom. 33 (2022) 31. ⟨https://surfacespectra.com/books/tof-sims/⟩.
[39] M.J. Graham, R.J. Hussey, Characterization and growth of oxide films, Corros. Sci. 44 (2002) 319, https://doi.org/10.1016/S0010-938X(01)00063-4.

[40] J. Jedlinski, A. Bernasik, K. Kowalski, M. Nocun, On the application of SIMS to study the oxidation mechanisms of alumina formers, Mater. High. Temp. 22 (2005) 505, https://doi.org/10.1179/mht.2005.061.
[41] A. Seyeux, G.S. Frankel, N. Missert, K.A. Unocic, L.H. Klein, A. Galtayries, P. Marcus, ToF-SIMS imaging study of the early stages of corrosion in Al-Cu thin films, J. Electrochem. Soc. 158 (2011) C165.
[42] M. Esmaily, P. Malmberg, M. Shahabi-Navid, J.E. Svensson, L.G. Johansson, ToF-SIMS Investigation of the Corrosion Behavior of Mg Alloy AM50 in Atmospheric Environments, Appl. Surf. Sci. 360 (2016) 98, https://doi.org/10.1016/j.apsusc.2015.11.002.
[43] N. Mortazavi, C. Geers, M. Esmaily, V. Babic, M. Sattari, K. Lindgren, P. Malmberg, B. Jönsson, M. Halvarsson, J.E. Svensson, I. Panas, L.G. Johansson, Interplay of water and reactive elements in oxidation of alumina-forming alloys, Nat. Mater. 17 (2018) 610, https://doi.org/10.1038/s41563-018-0105-6.
[44] K. Möller, Korrosion av koppar i rent syrefritt vatten, R-12-05, Swedish Nuclear Fuel and Waste Management Co, 2012, p. 31. R-12-05.
[45] K. Ollila, Copper Corrosion Experiments under Anoxic Conditions, R-13-34, Swedish Nuclear Fuel and Waste Management Co, 2013, p. 39. R-13-34.
[46] A.B. Belonoshko, A. Rosengren, Ab initio study of water interaction with a Cu surface, Langmuir 26 (2010) 16267.
[47] C.M. Lousada, A.J. Johansson, P.A. Korzhavyi, Thermodynamics of H_2O splitting and H_2 formation at the Cu(110)–water interface, J. Phys. Chem. C. 119 (2015) 14102.
[48] C.M. Lousada, A.J. Johansson, P.A. Korzhavyi, Molecular and dissociative adsorption of water at a defective Cu(110) surface, Surf. Sci. 658 (2017) 1.
[49] C.M. Lousada, A.J. Johansson, P.A. Korzhavyi, Adsorption of hydrogen sulfide, hydrosulfide and sulfide at Cu(110)—polarizability and cooperativity effects. First stages of formation of a sulfide layer, ChemPhysChem 19 (2018) 2159.
[50] A.J. Johansson, C. Lilja, T. Brinck, On the formation of hydrogen gas on copper in anoxic water, J. Chem. Phys. 135 (2011), 084709.
[51] N. Taniguchi, M. Kawasaki, Influence of sulfide concentration on the corrosion behavior of pure copper in synthetic seawater, J. Nucl. Mater. 379 (2008) 154.
[52] M.G. Ganchenkova, Y.N. Yagodzinskyy, V.A. Borodin, H. Hänninen, Effects of hydrogen and impurities on void nucleation in copper: simulation point of view, Philos. Mag. 94 (2014) 3522–3548.
[53] P.A. Korzhavyi, R. Sandström, Monovacancy in copper: trapping efficiency for hydrogen and oxygen impurities, Comput. Mater. Sci. 84 (2014) 122.
[54] C.M. Lousada, P.A. Korzhavyi, Hydrogen sorption capacity of crystal lattice defects and low Miller index surfaces of copper, J. Mater. Sci. 55 (2020) 6623.
[55] A.B. Belonoshko, A. Rosengren, A possible mechanism of copper corrosion in anoxic water, Philos. Mag. 92 (2012) 4618.
[56] C.M. Lousada, P.A. Korzhavyi, Segregation of P and S impurities to a Σ9 grain boundary in Cu, Metals 10 (2020) 1362.
[57] Y. Li, P.A. Korzhavyi, R. Sandström, C. Lilja, Impurity effects on the grain boundary cohesion in copper, Phys. Rev. Mater. 1 (2017), 070602.
[58] H. Magnusson, K. Frisk, Self-diffusion and impurity diffusion of hydrogen, oxygen, sulphur and phosphorus in copper, TR-13-24, Swed. Nucl. Fuel Waste Manag. (2013). ⟨https://www.skb.se/publication/2477839/TR-13-24.pdf⟩.